

Inter-comparisons of marine boundary layer cloud properties from the ARM CAP-MBL campaign and two MODIS cloud products

Zhibo Zhang^{1,2,*}, Xiquan Dong³, Baike Xi⁴, Hua Song², Po-Lun Ma⁵,

Steven J. Ghan⁵, Steven Platnick⁶, and Patrick Minnis⁷

1. Physics Department, UMBC, Baltimore, MD

2. Joint Center Joint Center for Earth Systems Technology (JCET), UMBC,

Baltimore, MD

3. Department of Hydrology and Atmospheric Sciences, University of Arizona,

Tucson, AZ.

4. Department of Atmospheric Sciences, University of North Dakota, Grand Forks,

ND

5. Pacific Northwest National Laboratory

6. NASA Goddard Space Flight Center, Greenbelt, MD

7. NASA Langley Research Center

For publication in JGR-Atmospheres, revised Dec. 2016.

* Corresponding Author: Zhibo Zhang (zzbatmos@umbc.edu)

22 **Abstract**

23 From April 2009 to December 2010, the Department of Energy (DOE) Atmospheric
24 Radiation Measurement (ARM) program carried out an observational field campaign on
25 Graciosa Island, targeting the marine boundary layer (MBL) clouds over the Azores
26 region. In this paper, we present an inter-comparison of the MBL cloud properties,
27 namely, cloud liquid water path (LWP), cloud optical thickness (COT) and cloud-droplet
28 effective radius (CER), among retrievals from the ARM mobile facility (AMF) and two
29 Moderate Resolution Spectroradiometer (MODIS) cloud products (GSFC-MODIS and
30 CERES-MODIS). A total of 63 daytime single-layer MBL cloud cases are selected for
31 inter-comparison. Comparison of collocated retrievals indicates that the two MODIS
32 cloud products agree well on both COT and CER retrievals, with the correlation
33 coefficient $R > 0.95$, despite their significant difference in spatial sampling. In both
34 MODIS products, the CER retrievals based on the 2.1 μm band ($\text{CER}_{2.1}$) is significantly
35 smaller than that based on the 3.7 μm band ($\text{CER}_{3.7}$). The GSFC-MODIS cloud product is
36 collocated and compared with ground-based ARM observations at several temporal-
37 spatial scales. In general, the correlation increases with more precise collocation. For the
38 63 selected MBL cloud cases, the GSFC-MODIS LWP and COT retrievals agree
39 reasonably well with the ground-based observations with no apparent bias and correlation
40 coefficient R around 0.85 and 0.70, respectively. However, GSFC-MODIS $\text{CER}_{3.7}$ and
41 $\text{CER}_{2.1}$ retrievals have a lower correlation ($R \sim 0.5$) with the ground-based retrievals. For
42 the 63 selected cases, they are on average larger than ground observations by about 1.5
43 μm and 3.0 μm , respectively. Taking into account that the MODIS CER retrievals are
44 only sensitive to cloud top reduces the bias only by 0.5 μm .

45

1. Introduction

Liquid-phase marine boundary layer (MBL) clouds cover approximately 20% of Earth's surface [Wood, 2012]. They are an important modulator of Earth's radiative energy budget [Klein and Hartmann, 1993]. A realistic and accurate representation of MBL clouds in general circulation models (GCM) is critical for understanding the global radiative energy budget, estimating aerosol indirect effects, and projecting future climate change. Evaluating and improving GCM simulated MBL clouds requires accurate monitoring of MBL cloud microphysical and optical properties, as well as their association with environmental factors such as meteorological conditions and aerosol loading.

The need for such observations motivated the Clouds, Aerosol, and Precipitation in the Marine Boundary Layer (CAP-MBL) field campaign funded by the U.S. Department of Energy (DOE) Atmospheric Radiation Measurement (ARM) Program [Wood *et al.*, 2014]. In this campaign, the ARM Mobile Facility (AMF) was deployed to Graciosa Island (39.09°N, 28.03°W) for 21 months from April 2009 to December 2010. Graciosa Island is part of the Azores archipelago in the eastern Atlantic. It is subject to a wide range of different meteorological conditions, mostly involving marine stratus and stratocumulus clouds [Wood *et al.*, 2014; Dong *et al.*, 2014a]. Thus, it is an ideal location for observing MBL clouds and studying how they are influenced by environmental factors, such as aerosol loading and large-scale circulation pattern. The ARM AMF instruments provide a variety of cloud and aerosol observations, as well as related

radiation fields and meteorological conditions. Recent studies have proven these observations to be a valuable data record for studying aerosol and cloud interactions in an otherwise poorly sampled remote marine environment [Logan *et al.*, 2014; Dong *et al.*, 2014a; 2014b].

In addition to ground-based ARM observations, satellite sensors, such as the Moderate Resolution Imaging Spectroradiometer (MODIS) on board of NASA's Terra and Aqua satellites, are another important source of cloud property observations. Among many operational and research-level MODIS-based cloud property products that have been developed, two are best recognized and most widely used. The first one is the "MOD06" product developed and maintained by a science team at NASA Goddard Space Flight Center (GSFC) [Platnick *et al.*, 2003; 2016]. It will be referred to as the "GSFC-MODIS product" hereafter. The other one is developed by a science team at NASA Langley Research Center, as part of the Clouds and Earth's Radiant Energy System (CERES) project [Minnis *et al.*, 2011b], which will be referred to as the "CERES-MODIS product" hereafter. Both products have been used in previous studies for evaluating the cloud simulations in GCMs [e.g., Kay *et al.*, 2012; Pincus *et al.*, 2012; Dolinar *et al.*, 2014].

Ground-based ARM cloud observations and satellite-based MODIS cloud products are two important sources for cloud related studies and for GCM evaluations. It is important to assess and understand the potential differences between the two datasets. Recently, Xi *et al.* [2014] (referred to as Xi14 hereafter) compared the MBL cloud properties from the ARM's Graciosa site during CAP-MBL campaign to the CERES-

MODIS cloud products for 63 daytime and 92 nighttime MODIS overpass cases. For collocation purposes, ground-based measurements are averaged over a one-hour window centered at the satellite overpass time, whereas the CERES-MODIS retrievals are averaged over a 30 km x 30 km box centered at the Graciosa ARM site (referred to as “dL30km-dt60min” averaging scheme). The ground- and satellite-based measurements agree well on the cloud-top temperature of MBL clouds. However, they have significant differences in other cloud properties, including cloud LWP, COT and CER. In particular, CERES-MODIS COT retrievals are on average smaller than their counterparts from ARM ground-based retrievals by about 4.1 or 30% ($R \sim 0.66$). On average, the CER retrievals from the CERES-MODIS $CER_{2.1}$ and $CER_{3.7}$ are larger than the ground-based retrievals by about $3.75 \mu\text{m}$ (30%) and $1.33 \mu\text{m}$ (10%), respectively ($R \sim 0.53$ and 0.49 , respectively). The underestimated COT and overestimated CER in the CERES-MODIS product lead to error cancellation and a rather small LWP difference, generally within 12%, in comparison with ground-based retrievals ($R \sim 0.62$). Overall, it was found that the ground- and satellite-based cloud properties at the Graciosa site do not agree as well as their continental low cloud counterparts at ARM’s SGP reported in *Dong et al.* [2008].

The differences between ground- and satellite-based cloud retrievals stem from two major sources. The first is the collocation uncertainty. Ground-based instruments make single-point observations, whereas satellite imagers like MODIS take instantaneous snapshots of a large area. In addition, all instruments have finite temporal and spatial resolutions. For example, the ground-based cloud retrievals have a nominal 5-minute temporal resolution [*Dong et al.*, 1998; *Xi et al.*, 2014]. *Xi14* is based on a dL30km-

dt60min collocation scale. Ideally, a smaller temporal-spatial averaging window would allow a more precise match between ground- and satellite-based observations. However, the sub-sampling scheme used by the CERES-MODIS algorithm leads to an effective spatial resolution of approximately 2.8 km. As a result, it is difficult to reduce the spatial averaging domain to a much smaller size than 30 km while maintaining enough statistics. It remains unclear whether a more precise temporal-spatial collocation would lead to a better agreement between ground- and satellite-based observations.

The second source is due to the differences in retrieval methods and algorithms. For example, the MODIS CER retrieval algorithm is based on the cloud reflection of solar radiation in the shortwave infrared (SWIR) spectral region (e.g., 2.1 μm and 3.7 μm). Because of the cloud absorption, the SWIR band had only limited penetration depth into the cloud top and therefore the MODIS CER retrieval is only sensitive to the cloud microphysics in the upper part of the cloud [Platnick, 2000; Zhang and Platnick, 2011]. In contrast, the ground-based CER retrieval is based on the surface solar transmission measurement and therefore is a vertically averaged CER [Dong *et al.*, 1997; Dong and Mace, 2010]. Another example is that the ground-based cloud LWP is directly retrieved from microwave radiometer (MWR) observations, whereas MODIS LWP is a diagnostic variable derived from the COT and CER retrievals.

Xi14 analyzed the potential reasons for the differences in LWP, COT and CER between ground-based retrievals and collocated CERES-MODIS retrievals, mainly from the perspective of differences in retrieval methods and algorithms. For example, they demonstrated in several cases that in comparison with the ground-based CER profile

retrievals, the CERES-MODIS CER retrievals based on different SWIR bands, i.e., 2.1 μm and 3.7 μm (hereafter referred to as CER_{2.1} and CER_{3.7}, respectively), are qualitatively aligned with theoretical expectations, i.e., CER_{2.1} penetrates deeper into the cloud than CER_{3.7}. Their investigation into the impacts of collocation uncertainty was limited by the sub-sampling scheme of the operational CERES-MODIS cloud retrieval algorithm. Although most MODIS bands have a nominal resolution of 1 km, the CERES-MODIS cloud retrieval algorithm only sub-samples every fourth pixel and every other scan line of the 1 km MODIS measurements [Minnis *et al.*, 2011a]. As such, there is only a one eighth probability that the CERES-MODIS near-site pixel includes the site in its field of view. In some cases, the nearest CERES-MODIS pixel center may be as far as 10 km from the site. As a result, it remains unclear if the differences between ground-based and CERES-MODIS cloud properties are mainly due to differences in retrieval algorithm or collocation uncertainty.

This study is a follow-up to *Xi14*. In addition to the CERES-MODIS product, we introduce another MODIS product—the GSFC-MODIS cloud product—in the comparison with ground-based observations. As explained later, the GSFC-MODIS cloud product samples every 1 km MODIS observation, which enables a better temporal-spatial collocation with the ARM ground site. We first compare the pixel-level cloud properties, including cloud LWP, COT and CER, from the two MODIS products with ground-based measurements for the 63 daytime overpass cases reported in *Xi14*. In addition, we also compare the monthly mean (i.e., level-3) MODIS cloud product with the aggregated ground-based measurements during the 19-month CAP-MBL campaign period.

One objective of this study is to better understand to what extent the ground- and satellite-based retrievals of MBL cloud properties agree with one another so that they can be used with greater confidence for evaluating and improving the MBL cloud simulations in GCMs. The rest of this paper is organized as follows. Section 2 provides an overview of the ground-based and satellite-based cloud properties retrievals used for the inter-comparison. The comparison results for the 63 collocated MODIS overpass cases are presented and discussed in Section.3.

2. Ground- and satellite-based measurements and retrievals

2.1. Ground-based cloud properties from ARM CAP-MBL campaign

2.1.1. Cloud LWP retrievals from MWR

The ground-based cloud LWP product used in the inter-comparison is derived from the MWR measurements at the ARM Graciosa site during the CAP-MBL campaign. The ARM MWR measures the downwelling brightness temperatures (BT) at surface at 23.8 and 31.4-GHz. Water vapor emission dominates the signal in the 23.8-GHz channel, whereas liquid water emission constitutes the primary portion of the signal at 31.4 GHz. *Liljegren et al.* [2001] developed a statistical retrieval method to retrieve both LWP and total precipitable water vapor (PWV) simultaneously from the dual frequency BT measurements. This algorithm is simple, computationally fast and has been adopted as the operational LWP and PWV retrieval algorithm for ARM MWR. Its main limitation is that the retrieval parameters required in this algorithm are based on a statistical fitting of the measured BT to the simulated BT from radiative transfer model. As a result, the

instantaneous retrievals from this algorithm may be subject to significant uncertainties, approximately 25 g/m^2 for LWP and 0.5 mm for PWV (<http://www.arm.gov/instruments/mwr>).

Instantaneous MWR retrievals are known to be noisy due to broken clouds and/or retrieval uncertainties. For better data quality, the instantaneous MWR LWP retrievals ($\sim 20\text{s}$ frequency) are aggregated to 5-minute intervals. Cloud fractions and boundary retrievals from ARM's active sensors, including ceilometer and cloud profiling radar, are used during the aggregation to screen out clear-sky and overlapping cloud conditions. Namely, MWR LWP retrievals are aggregated only when active sensors detect overcast single-layer low clouds within a 5-minute period. Therefore, the MWR LWP retrievals for the 63 selected cases used in the inter-comparison are averaged *in-cloud* LWP with a 5-minute frequency.

2.1.2. CER and COT retrievals based on Dong et al. [1998] parameterization scheme

The ground-based cloud CER and COT property retrievals for MBL clouds are based on the algorithm described in Dong et al. [1997; 1998]. The inputs to the algorithm include the abovementioned aggregated 5-minute LWP retrieval from the MWR and the downwelling solar flux at the surface from ground pyranometer measurements. Dong et al. [1998] developed a simple CER parameterization scheme, which has proven to provide equally accurate CER retrievals as the interactive scheme in Dong et al. [1997]. The scheme is as follows:

$$\overline{CER}(LWP, \gamma) = -2.07 + 2.49LWP + 10.25\gamma - 0.25\mu_0 + 20.28LWP \cdot \gamma - 3.14LWP \cdot \mu_0 \quad (1)$$

where LWP is from the MWR, μ_0 is the cosine of solar zenith angle and $\gamma = F_{cloudy}^{\downarrow} / F_{clear}^{\downarrow}$ is the ratio of measured cloudy-sky downwelling solar flux (F_{cloudy}^{\downarrow}) to the expected clear-sky downwelling solar flux (F_{clear}^{\downarrow}) when there were no clouds [Long and Ackerman, 2000]. The upper-bar in \overline{CER} indicates that the retrieval is based on the vertically homogeneous cloud assumption and \overline{CER} can be considered as an effective vertical average of the CER profile. A new algorithm developed by Dong and Mace [2010] and Dong et al. [2014b] to retrieve the profiles of CER and LWC, is overviewed in the next section.

2.1.3. CER and LWC profile retrievals

As explained above, the retrievals based on Dong et al. [1998] can be considered as a vertically averaged CER. Dong and Mace [2010] developed a new retrieval scheme that combines the radar reflectivity profile ($Z(h)$) from the K-band (35GHz) millimeter wavelength radar (MMCR), LWP from MWR, and pyranometer γ measurements to retrieve the vertical profile of CER and liquid water content (LWC) of MBL clouds. On the basis of the log-normal particle size distribution (PSD) assumption and the analytical relations between radar reflectivity and PSD, Dong and Mace [2010] related the vertical profile of CER to the $Z(h)$ profile from MMCR and the vertically averaged CER based on Dong et al. [1998] as follows:

217

$$218 \quad CER(h) = \overline{CER} \cdot \left[\frac{\Delta H}{\Delta h} \frac{Z^{1/2}(h)}{\sum_{base}^{top} Z^{1/2}(h)} \right]^{1/3} \quad (2)$$

219 where \overline{CER} is from the *Dong et al.* [Dong et al., 1998] parameterization scheme in Eq.(1)
 220 , ΔH is the physical thickness of the MBL cloud, and Δh is the MMCR range gate
 221 spacing. Once $CER(h)$ is known from Eq.(2) , other key cloud properties such as the
 222 LWC profile, can be easily derived from $CER(h)$ and the assumed PSD.

223 2.2. GSFC-MODIS and CERES-MODIS cloud products

224 In this study, we use the latest Edition-4 CERES-MODIS product [Minnis et al.,
 225 2011b; 2011c] and the collection 6 GSFC-MODIS cloud product [Platnick et al., 2016].
 226 Both MODIS cloud products use the so-called bi-spectral method to simultaneously
 227 retrieve COT and CER from cloud reflectance measurements in two spectral bands
 228 [Nakajima et al., 1990]. One measurement is usually made in the visible or near-infrared
 229 (VIS/NIR) spectral region (e.g., 0.64 μm or 0.86 μm), where water absorption is
 230 negligible and therefore cloud reflection generally increases with COT. The other
 231 measurement is usually in the shortwave infrared (SWIR) spectral region (e.g., 2.1 or 3.7
 232 μm), where water droplets are moderately absorptive and cloud reflectance generally
 233 decreases with increasing CER for optically thick clouds. Once the COT and CER are
 234 determined using the bi-spectral method, the LWP can be derived from the equation
 235 $LWP = 2 / 3 \rho_w COT \cdot CER$.

236 MODIS has three SWIR bands centered at 1.6, 2.1 and 3.7 μm , respectively,
237 which can all be used for CER retrieval in the bi-spectral method. Both MODIS cloud
238 products report the CER retrievals based on the 2.1 μm and 3.7 μm retrievals (i.e., $\text{CER}_{2.1}$
239 and $\text{CER}_{3.7}$). In addition, the GSFC-MODIS also reports the $\text{CER}_{1.6}$. A number of recent
240 studies found significant differences between $\text{CER}_{2.1}$ and $\text{CER}_{3.7}$ in the GSFC-MODIS
241 and CERES-MODIS products for MBL clouds [Nakajima *et al.*, 2010; Painemal and
242 Zuidema, 2011; Zhang and Platnick, 2011; Zhang *et al.*, 2012]. Sub-pixel cloud
243 inhomogeneity is an important reason causing this spectral difference [Zhang and
244 Platnick, 2011; Zhang *et al.*, 2012]. Note that when $\text{CER}_{2.1}$ and $\text{CER}_{3.7}$ are used to derive
245 the LWP, the retrievals are referred to as $\text{LWP}_{2.1}$ and $\text{LWP}_{3.7}$, respectively.

246 A major difference between the two MODIS cloud products is in their spatial
247 sampling scheme. The CERES-MODIS product is developed mainly to facilitate the
248 CERES measurements of the top-of-atmosphere (TOA) radiation [Minnis *et al.*, 2004;
249 2011b]. The CERES scanners on Terra and Aqua have a nadir spatial resolution of ~ 20
250 km. They rely on the high-resolution MODIS observations to identify the atmospheric
251 and surface components within the CERES field of view (FOV) so that the measured
252 CERES broadband radiances can be converted into fluxes [Loeb *et al.*, 2005]. In order to
253 minimize the processing time, the CERES-MODIS retrieval algorithm sub-samples every
254 fourth pixel and every other scan line of the 1-km MODIS measurements. As a result, the
255 CERES-MODIS cloud product has an effective spatial resolution of 2.8 km. Thus, there
256 are approximately 50 CERES-MODIS cloud retrievals in a 20-km CERES footprint. The
257 operational level-2 CERES-MODIS cloud retrieval product is released together with the

CERES TOA radiation measurements in the CERES- Single Scanner Footprint (SSF) product[†]. For each 20-km CERES footprint in the data, the corresponding cloud property statistics, such as mean and standard deviation, are reported based on the ~50 subsampled MODIS retrievals. For CERES Edition 4, the individual subsampled CERES-MODIS pixel retrievals are also archived for additional analyses. The pixel retrievals for a 30 km x 30 km box centered on the ARM site were used in *Xi14*.

In contrast to the CERES-MODIS sub-sampling scheme, in the latest collection 6 of the GSFC-MODIS cloud product, the CER and COT retrievals are attempted for every possible 1-km cloudy pixel. The retrieval results for overcast and potentially partly cloudy pixels are reported separately in the product to reflect their difference in terms of retrieval quality.

3. Inter-comparison Results for *Xi14* cases

The polar orbit and the wide cross-track swatch (2330 km) enable each MODIS to sample the Graciosa site on daily basis (once most days and some days twice). **Figure 1**, plots the Aqua- and Terra-MODIS swath overpass times for Graciosa Island during the CAP-MBL campaign period. The overpass time for Aqua is mostly between 14:00 and 16:00 UTC, while it is mostly between 12:00 and 14:00 UTC for Terra. During the whole CAP-MBL campaign period, each MODIS made over 830 daytime observations over Graciosa Island. However, most of these overpasses are not ideal for inter-comparison purpose because the area is either cloud-free or not covered by single-layer MBL clouds (e.g., covered by ice cloud or overlapping clouds). Indeed, *Xi14* only found 63

[†] https://eosweb.larc.nasa.gov/project/ceres/ssf_table

overpassing cases, in which the Graciosa Island region—a 30 km x 30 km box centered at ARM AMF site—is covered by single-layered overcast MBL clouds according to the CERES-MODIS cloud product.

It should be mentioned that when using the 1-km GSFC-MODIS cloud mask product to derive the cloud fraction in the same region, a number of scenes in the 63 cases are actually not overcast (cloud fractions as low as 60%) but the ARM MMCR and lidar observations show a continuous cloud layer. This difference may be due to the sub-sampling scheme of the CERES-MODIS cloud product, leading to an overestimation of cloud fraction in some mostly cloudy scenes when the cloud-free pixels may not be sampled. Nevertheless, the inter-comparison results indicate that the difference of cloud fraction between the two MODIS cloud products has little impact on the comparison. We start our inter-comparison with these cases because they are relatively simple and also because our results are directly comparable with those reported in *Xi14*.

3.1. Comparison of GSFC- and CERES-MODIS products

Before exploring the differences between ground-based cloud retrievals with the MODIS cloud results, we first compare the two MODIS cloud products. For collocation, we first identify in the level-2 CERES-SSF product the CERES footprint closest to the ARM's AMF site on the Graciosa Island. Then, we found all the 1-km pixels of the GSFC-MODIS cloud retrievals within the 20 km CERES footprint as identified in the previous step. Finally, we averaged the GSFC-MODIS cloud retrievals from all the cloudy pixels within the CERES footprint and compared them with the averaged CERES-

MODIS values reported in the CERES-SSF product that are based on the ~50 sub-sampled pixels.

Figure 2 shows the comparisons of COT, $CER_{3.7}$ and $CER_{2.1}$ between the collocated CERES-MODIS and GSFC-MODIS for the 63 *Xi14* cases. The gray scale of the dots corresponds to the cloud fraction over the 30 km x 30 km box centered at ARM AMF site according to the GSFC-MODIS 1 km cloud mask product. Evidently, the two products are in close agreement, regardless of the cloud fraction. The correlation coefficients for COT and $CER_{3.7}$ are both 0.95 and there is no apparent systematic bias between the two products. This is very encouraging even though the comparison is based on limited cases.

What is a little surprising is that the $CER_{2.1}$ retrievals from the CERES-MODIS product are systematically larger than their GSFC-MODIS counterparts in **Figure 2c**, although the correlation efficient remains as high as 0.93. This difference appears to be greater for larger CER values and could be partially due to small differences in the C5 and C6 Terra 2.1- μ m calibrations used by the CERES-MODIS and GSFC-MODIS analyses. Because of the non-linear relationship between reflectance and $CER_{2.1}$, a given fractional change in the reflectance, equivalent to a change in the calibration gain, will cause a much larger change in $CER_{2.1}$ for large droplets than for small droplets. Differences in the treatment of atmospheric absorption or in the modeling of the top-of-atmosphere reflectances could also account for the size-dependent $CER_{2.1}$ difference between CERES-MODIS and GSFC-MODIS. This result implies that there is a larger difference between $CER_{3.7}$ and $CER_{2.1}$ in the CERES-MODIS product than in the GSFC-

MODIS product, which is confirmed in **Figure 3**. In the GSFC-MODIS product (**Figure 3a**), the $CER_{2.1}$ is larger than $CER_{3.7}$ for all but one case. The results in **Figure 3b** indicate that the CERES-MODIS product has the same issue. The magnitude of the spectral difference is even larger.

As explained in several previous studies, sub-pixel cloud inhomogeneity (SPI) is an important reason causing the spectral difference between $CER_{3.7}$ and $CER_{2.1}$ [e.g., *Zhang and Platnick, 2011; Painemal et al., 2012; Zhang et al., 2012*]. To examine the dependence of the spectral difference between $CER_{3.7}$ and $CER_{2.1}$ on SPI, we colored each case in **Figure 3** based on the mean SPI index of the MBL cloud pixels in each case from the GSFC-MODIS product. This SPI index product is derived from the 250m sub-pixel variance of cloud reflectance, which is close to zero for highly homogeneous cloud and up to about 1.0 for highly inhomogeneous clouds. In general, we see that the cases with larger SPI (darker dots) tend to have larger spectral difference between $CER_{2.1}$ and $CER_{3.7}$ than those with more homogeneous cases with smaller SPI (lighter dots). Similar results were found by *Painemal et al. [2013]* using the 2.8-km CERES-MODIS data to estimate horizontal homogeneity.

The dependence on SPI index is further examined in **Figure 4**. The background color map of the figure corresponds to the mean $CER_{2.1}-CER_{3.7}$ at each combination of SPI index and $CER_{2.1}$ derived from the total population of GSFC-MODIS pixels from all 63 *Xi14* cases. The dotted contour lines correspond to the relative sampling rate (the center contour line has the largest sampling rate). Each dot in the figure corresponds to one of the 63 *Xi14* cases. The location of the dots on x- and y-axis corresponds to the

mean value of SPI index and $CER_{2.1}$ of each case, respectively. The color of each dot corresponds to the mean $CER_{2.1}-CER_{3.7}$ value of each case. The background color pattern in **Figure 4** reveals a rather complicated dependence of $CER_{2.1}-CER_{3.7}$ on both SPI index and $CER_{2.1}$, which is a manifestation of multiple mechanisms operating at the same time and entangled with one another [Zhang and Platnick, 2011; Zhang et al., 2012]. Nonetheless, a general pattern in **Figure 4** is that, in the region with relatively high sampling rate, the $CER_{2.1}-CER_{3.7}$ difference tends to increase with increasing SPI index as a result of the aforementioned PPHB. It is encouraging to see the color of the dots, which is based on the mean value of $CER_{2.1}-CER_{3.7}$ in each case, is in general agreement of the background color based on the total population of pixels from all 63 cases. Overall, the results in **Figure 3** and **Figure 4** suggest that the PPHB plays an important role in causing the size difference between $CER_{2.1}$ and $CER_{3.7}$ for the *Xi14* cases.

In summary, the COT and $CER_{3.7}$ retrievals from the CERES-MODIS product agree well with their GSFC-MODIS counterparts for the 63 MBL cloud cases studied here. In both products, the $CER_{2.1}$ retrievals are systematically larger than the $CER_{3.7}$ retrievals. This spectral difference is more severe in the CERES-MODIS product than in the GSFC-MODIS product. As a result, the CERES-MODIS $CER_{2.1}$ retrievals are systematically larger than those from GSFC-MODIS. The PPHB is likely to be an important reason causing the spectral difference between $CER_{2.1}$ and $CER_{3.7}$.

3.2. Comparisons of ARM ground-based retrievals with the GSFC-MODIS product

In this section, we focus on the comparison between ground-based cloud retrievals with the GSFC-MODIS product. We do *not* include CERES-MODIS product in the comparison for two reasons. First, as shown in the last section the two MODIS cloud products are in excellent agreement, which implied that whatever lessons are learned from the comparison about the GSFC-MODIS product should also apply to the CERES-MODIS product. Second, as mentioned in section 0, because of the sub-sampling scheme of CERES-MODIS retrieval algorithm and how the retrieval results are organized and reported in the CERES-SSF product, it is difficult to make precise collocation between the CERES-MODIS retrievals and ground measurements. For this reason the Xi14 used the “dL30km-dt60min” averaging scheme. Because the GSFC-MODIS algorithm attempts retrieval for every 1-km pixel, it has a spatial sampling rate about 8 times higher than the CERES-MODIS cloud product. This provides us an opportunity to investigate if closer temporal-spatial matching yields better agreement between ground- and satellite-based cloud retrievals. For this purpose, we developed a total of 9 matching conditions based on the cross combinations of 3 spatial averaging dimensions dL= 30, 20 and 10 km and 3 temporal averaging windows dt = 60, 30 and 10 minutes. Therefore, we focus on the GSFC-MODIS product in the comparisons that follow.

Figure 5 shows the results from LWP comparison. As shown in **Figure 5a** and **5b** when we use the dL30km-dt60min averaging scheme, the correlation coefficient between the ground-based MWR LWP retrievals and the corresponding GSFC-MODIS LWP

retrievals product is about 0.62 for the 63 *Xi14* cases. This value is identical to that
 reported in *Xi14* based on the CERES-MODIS product (see their Figure 8c), which is
 expected, given the excellent agreement between the two MODIS products. To explore
 the sensitivity to matching conditions, we progressively reduced the temporal-spatial
 averaging window in 9 sensitivity tests. The resulting correlation coefficients from these
 tests are listed in Table 1. Apparently, the correlation between ground- and satellite-based
 LWP keeps increasing with decreasing temporal-spatial averaging window, from the
 lowest value of about 0.62 for dL30km-dt60min (**Figure 5a** and 5b) to the highest value
 of about 0.85 for dL10km-dt10min (**Figure 5c** and 5d). This is aligned with the
 expectation that closer collocation leads to better agreement between ground- and
 satellite-based retrievals. The small arrow in **Figure 5** marks a prominent and interesting
 case that attests the importance of close collocation for matching ground- and satellite-
 based observations. This case was observed on May 14th, 2010 around 12:50 UTC.
Figure 6 shows the RGB image of this case from the Terra-MODIS. Zooming in on
 Graciosa Island, one can find that the island is covered by thick MBL clouds while the
 surrounding region is either clear or covered by thinner clouds. While this could be due to
 island effects or simply a coincidence, it is evident that a dL30km averaging range would
 include a large fraction of thin clouds around the island. As a result the mean satellite-
 based LWP in **Figure 5a** and 5b is quite low, only $\sim 40 \text{ g/m}^2$, while the ground-based
 LWP is almost 8 times larger at $\sim 320 \text{ g/m}^2$. Reducing the temporal-spatial averaging
 window to dL10km-dt10min (**Figure 5c** and 5d) significantly increases the satellite-
 based LWP and also reduces the ground-based LWP, leading to a much closer agreement.

408 The presence of precipitation in MBL clouds poses challenges to both MWR and
409 MODIS LWP retrievals. The current operational MWR retrieval algorithm considers only
410 the absorption effect of cloud water and ignores the scattering effect. This assumption can
411 be problematic for drizzling MBL clouds, because the drizzle drops are large enough to
412 have significant scattering in MWR wavelength [*Liljegren et al.*, 2001]. The difficulties
413 in retrieving cloud water when drizzle is present using microwave sensors are discussed
414 in *Lebsock and L'Ecuyer* [2011] and *Lebsock et al.* [2011]. For MODIS retrieval, the
415 changes of vertical structure and microphysics (e.g., bi-modal PSD) caused by the warm
416 rain process can make the properties of drizzling MBL clouds deviate from the
417 fundamental assumptions made in the operational MODIS algorithm and results in
418 significant uncertainty [*Seethala and Horváth*, 2010; *Lebsock and Su*, 2014; *Miller et al.*,
419 2016]. In **Figure 5**, we marked each case with a gray scale according to the fraction of
420 precipitation during the temporal averaging window based on the MMCR observations. A
421 case with darker color indicates a larger fraction of MBL clouds observed by the MWR
422 during the temporal averaging window are precipitating. As expected, the cases with
423 larger precipitation fraction (i.e., darker dots) generally have larger mean LWPs than
424 those with mostly non-precipitating clouds. Interestingly, the comparison between
425 ground-based and GSFC-MODIS LWP retrievals show no apparent dependence on the
426 precipitation fraction because the light drizzle cases used in *Xi14* to have little impact on
427 the LWP retrievals. Further investigation is needed to better understand the impacts of
428 drizzle on the MWR and MODIS retrievals and their differences.

429 Given the LWP comparisons, we now compare COT and CER values. **Figure 7**
 430 shows comparisons of the GSFC-MODIS COT, CER_{2.1} and CER_{3.7} values with their
 431 ground-based counterparts based on the *Dong et al.* [1998] parameterization described in
 432 section 2.1.2. As in **Figure 5**, the gray scale in **Figure 7** indicates the fraction of
 433 precipitation during the temporal averaging window based on the MMCR observations.
 434 When the dL30km-dt60min averaging scheme is used, the correlation coefficient
 435 between ground- and satellite-based COT retrievals for the 63 *Xi14* cases is 0.62, which
 436 is consistent with the CERES-MODIS results in *Xi14* and also comparable to the
 437 correlation coefficient for LWP in **Figure 5a** and **5b**. The ARM retrievals seem to be
 438 systematically higher than the GSFC-MODIS COT retrievals, as found in *Xi14*. Indeed
 439 the P-value based on the T-test is only 0.04 for the null hypothesis test that the two COT
 440 data sets have the same mean value. When the averaging window is reduced to dL10km-
 441 dt10min, the correlation coefficient for COT increases slightly to 0.7, which is
 442 encouraging but not as significant as that seen in **Figure 5** for LWP. The *P*-value also
 443 increases to 0.89, indicating that smaller averaging window helps to reduce the bias. The
 444 CER comparisons between the GSFC-MODIS and ARM retrievals using the dL10km-
 445 dt10min scheme, on the other hand, have nearly the same correlations as those using the
 446 dL30km-dt60min averaging scheme but larger mean differences and standard deviations.
 447 The LWP, COT and CER comparisons have demonstrated that the dL10km-dt10min
 448 scheme can increase the correlation but does not always diminish the satellite-surface
 449 differences as shown in *Dong et al.* [2008]. This is primarily due to mismatch between

the surface temporal averages and satellite spatial averages and uncertainties in the two retrieval methods.

Figure 7 also compares the GSFC-MODIS CER_{2.1} and CER_{3.7} retrievals with the *Dong et al.* [1998] ground-based CER retrievals. When the dL30km-dt60min averaging scheme is used, the correlation coefficient for CER_{3.7} and CER_{2.1} is 0.50 (**Figure 7b**) and 0.55 (**Figure 7c**), respectively. More importantly, based on the average of the 63 cases, CER_{3.7} and CER_{2.1} are 1.3 and 2.9 μm larger, respectively, than the *Dong et al.* [1998] ground-based CER averages, indicating the existence of systematic bias. Unlike the LWP and COT comparisons, the comparison of CER do not show any significant improvement when the averaging window drops to dL10km-dt10min (**Figure 7e** and **7f**). The correlation coefficient remains low around 0.5 and the bias even increases slightly.

In contrast to column-integrated variables like LWP and COT, CER is dependent on the vertical structure of MBL clouds. As mentioned in Section 2, the MODIS CER retrievals are only sensitive to the upper portion of the MBL clouds, while the ground-based CER retrievals from *Dong et al.* [1998] can be considered as the vertical average of the CER profile. Could this be the primary reason causing the differences between ground- and satellite-based CER retrievals seen in **Figure 7**? The ground-based CER and LWC profile retrievals from *Dong and Mace* [2010] provide the observations needed to address this question. To illustrate and quantify the sensitivity of MODIS CER retrieval to cloud vertical structure, *Platnick* [2000] introduced the concept of a vertical weighting function $W(\tau)$, which relates the MODIS CER retrieval with the vertical profile of CER as follows:

$$CER^* = \int_0^{COT} CER(\tau)W(\tau)d\tau \quad (3)$$

where τ is the optical depth from cloud top, $CER(\tau)$ is the CER profile as a function of τ . $W(\tau)$ is normalized so that $\int_0^{COT} W(\tau)d\tau = 1$. Given a CER profile, the computation of $W(\tau)$ involves rather expensive radiative transfer simulations. In this study, we adopt the concept of the vertical weighting function, but use an analytical form that can serve as a first order approximation to the actual weighting function to avoid expensive radiative transfer simulations:

$$W(\tau) = a\tau^b \exp\left[-\tau\left(\frac{1}{\mu} + \frac{1}{\mu_0}\right)\right] \quad (4)$$

where μ and μ_0 are the cosines of viewing and solar zenith angles, respectively, the exponent b determines the location of the maximum sensitivity, and a is a constant to ensure $W(\tau)$ is normalized. Because of the stronger cloud absorption in the 3.7- μm band, we let $b=0$ to approximately reduce $W(\tau)$ to the two-way transmittance [Alexandrov *et al.*, 2012; Miller *et al.*, 2016]. Meanwhile, we use $b=2$ for the $CER_{2.1}$ to allow a deeper penetration depth. A hypothetical example to demonstrate the use of the analytical weighting function is given in **Figure 8**. For this particular case, the $CER_{3.7}$ and $CER_{2.1}$ retrieval results predicted based on our analytical $W(\tau)$ are in reasonable agreement with the numerical simulations, although biased a little higher, lending confidence to our analytical $W(\tau)$ in Eq.(4).

To account for the sensitivity of the MODIS CER retrievals to cloud vertical structure in the comparison, we first use the LWC and CER profiles from the *Dong and Mace* [2010] scheme that are described in Section 2.1.3 to derive the vertical profile of CER as a function of optical depth, i.e., $CER(\tau)$. Then, we use the analytical $W(\tau)$ to derive from Eq. what the MODIS $CER_{3,7}$ and $CER_{2,1}$ retrieval results would be if the MODIS instrument had observed a MBL cloud with the given LWC and CER profiles (referred to as the “ARM vertically weighted” retrievals). Finally, we compare the ARM vertically weighted CER with the GSFC-MODIS retrievals in **Figure 9**. In comparison to the results in **Figure 7**, the vertical weighting helps to reduce the MODIS CER bias by $\sim 0.5 \mu\text{m}$ for both dL30km-dt60min and dL10km-dt10min averaging schemes. These results are consistent with the theoretical expectation. Nonetheless, there are still significant differences between ground- and satellite-based results. Depending on which averaging scheme is used, the GSFC-MODIS $CER_{3,7}$ retrievals for the 63 *Xi14* cases are about 0.9 to 1.5 μm larger than the ground-based CER retrievals, even if the MODIS CER retrieval sensitivity to the cloud vertical structure is considered. The $CER_{2,1}$ retrievals are even larger (by about 2.3 to 2.6 μm).

4. Conclusions and Discussion

The DOE ARM Program carried out a 19-month observation field campaign from April 2009 to December 2010—the CAP-MBL—on Graciosa Island (39° 5' 28" N, 28° 1' 45" W), targeting MBL clouds over the Azores. Here, we present an inter-comparison of the MBL cloud LWP, COT and CER between the CAP-MBL ARM AMF retrievals and

two satellite remote sensing products (CERES-MODIS and GSFC-MODIS). The main results from the comparison are summarized as follows:

- The two MODIS products show good agreement on COT and $CER_{3.7}$ (correlation coefficient $R \sim 0.95$). The $CER_{2.1}$ from CERES-MODIS product is systematically larger than that from GSFC-MODIS possibly due to calibration and/or algorithmic differences. In both MODIS products, MBL $CER_{2.1}$ tends to be larger than $CER_{3.7}$. The magnitude of $CER_{2.1} - CER_{3.7}$ increases with cloud sub-pixel inhomogeneity, suggesting that the plane-parallel homogeneous bias likely plays an important role in the spectral retrieval differences.
- Comparison between the ARM ground-based cloud retrievals and the GSFC-MODIS product depend on how the two datasets are collocated. A more precise collocation generally leads to better agreement. We found no systematic bias between the ground-based MWR and GSFC-MODIS LWP values. The correlation coefficient is about 0.85 for the 63 selected cases when using a more strict collocation scheme (dL10km-dt10min), while R reduces to 0.62 when using a more relaxed collocation scheme (dL30km-dt60min). Similarly, the ground- and satellite-based COT retrievals also agree reasonably well, with no apparent bias and correlation coefficient $R \sim 0.70$.
- Averaging over the 63 selected cases, the GSFC-MODIS $CER_{2.1}$ and $CER_{3.7}$ are about $1.5 \mu m$ and $3.0 \mu m$ larger than ground-based retrievals based on the *Dong et al.* [1998] scheme. Taking into account that the satellite-based CER retrievals

532 are only sensitive to cloud top reduces this bias by $\sim 0.5 \mu\text{m}$. Precipitation seems
533 to have little impact on the comparison.

534 These findings have several implications. First, the good agreement on instantaneous
535 retrievals should lend confidence to both MODIS products. They can be deemed to be
536 practically equivalent for studying the climatology of MBL clouds or evaluating the MBL
537 cloud simulations in GCMs. The fact that $\text{CER}_{2.1}$ is systematically larger than $\text{CER}_{3.7}$ in
538 both MODIS products indicates this spectral difference unlikely to be an algorithm issue,
539 but caused by more fundamental issues like sub-pixel level cloud inhomogeneity.

540 Second, in comparison with *Xi14*, a more precise temporal-space collocation in this study
541 leads to a better agreement between ground- and satellite-based retrievals of LWP and
542 COT. Together, the ARM and MODIS cloud property retrievals constitute a strong
543 constraint on the bulk physical and optical properties of MBL clouds over the Azores
544 region that should be highly useful for GCM evaluation. Finally, the differences between
545 the ground- and satellite-based CER indicate the existence of significant uncertainty in
546 the current observations of MBL cloud microphysics. Although the cause is yet to be
547 understood, this study provides a quantitative assessment of this uncertainty, which could
548 still be helpful for evaluating the GCM simulations of MBL clouds. This study is based
549 on limited cases. Now the ARM program has established a permanent site on the
550 Graciosa Island for long-term observations. We will extend our comparisons to the new
551 data record in future studies.

552

553

554 **Reference:**

- 555 Alexandrov, M. D., B. Cairns, C. Emde, A. S. Ackerman, and B. van Dierenhoven
 556 (2012), Accuracy assessments of cloud droplet size retrievals from polarized
 557 reflectance measurements by the research scanning polarimeter, *Remote Sensing of*
 558 *Environment*, 125(0), 92–111, doi:10.1016/j.rse.2012.07.012.
- 559 Dolinar, E. K., X. Dong, B. Xi, J. H. Jiang, and H. Su (2014), Evaluation of CMIP5
 560 simulated clouds and TOA radiation budgets using NASA satellite observations,
 561 *Climate Dynamics*, 44(7-8), 2229–2247, doi:10.1007/s00382-014-2158-9.
- 562 Dong, X., and G. G. Mace (2010), Profiles of Low-Level Stratus Cloud Microphysics
 563 Deduced from Ground-Based Measurements, [http://dx.doi.org/10.1175/1520-](http://dx.doi.org/10.1175/1520-0426(2003)020<0042:POLLSC>2.0.CO;2)
 564 [0426\(2003\)020<0042:POLLSC>2.0.CO;2](http://dx.doi.org/10.1175/1520-0426(2003)020<0042:POLLSC>2.0.CO;2), 20(1), 42–53, doi:10.1175/1520-
 565 [0426\(2003\)020<0042:POLLSC>2.0.CO;2](http://dx.doi.org/10.1175/1520-0426(2003)020<0042:POLLSC>2.0.CO;2).
- 566 Dong, X., B. Xi, A. Kennedy, P. Minnis, and R. Wood (2014a), A 19-Month Record of
 567 Marine Aerosol–Cloud–Radiation Properties Derived from DOE ARM Mobile
 568 Facility Deployment at the Azores. Part I: Cloud Fraction and Single-Layered MBL
 569 Cloud Properties, <http://dx.doi.org/10.1175/JCLI-D-13-00553.1>, 27(10), 3665–3682,
 570 doi:10.1175/JCLI-D-13-00553.1.
- 571 Dong, X., B. Xi, and P. Wu (2014b), Investigation of the Diurnal Variation of Marine
 572 Boundary Layer Cloud Microphysical Properties at the Azores, *J. Climate*, 27(23),
 573 8827–8835, doi:10.1175/JCLI-D-14-00434.1.
- 574 Dong, X., P. Minnis, B. Xi, S. Sun Mack, and Y. Chen (2008), Comparison of CERES -
 575 MODIS stratus cloud properties with ground-based measurements at the DOE ARM
 576 Southern Great Plains site, *J. Geophys. Res.*, 113(D3), D03204,
 577 doi:10.1029/2007JD008438.
- 578 Dong, X., T. P. Ackerman, and E. E. Clothiaux (1998), Parameterizations of the
 579 microphysical and shortwave radiative properties of boundary layer stratus from
 580 ground-based measurements, *J. Geophys. Res.*, 103(D24), 31681–31693,
 581 doi:10.1029/1998JD200047.
- 582 Dong, X., T. P. Ackerman, E. E. Clothiaux, P. Pilewskie, and Y. Han (1997),
 583 Microphysical and radiative properties of boundary layer stratiform clouds deduced
 584 from ground-based measurements, *J. Geophys. Res.*, 102(D20), 23829–23843,
 585 doi:10.1029/97JD02119.
- 586 Kay, J. E. et al. (2012), Exposing Global Cloud Biases in the Community Atmosphere
 587 Model (CAM) Using Satellite Observations and Their Corresponding Instrument
 588 Simulators, *Journal of Climate*, 25(15), 5190–5207, doi:10.1175/JCLI-D-11-
 589 00469.1.
- 590 Klein, S., and D. Hartmann (1993), The seasonal cycle of low stratiform clouds, *Journal*

591 *of Climate*, 6(8), 1587–1606.

592 Lebsock, M. D., and T. S. L'Ecuyer (2011), The retrieval of warm rain from CloudSat, *J*
593 *Geophys Res*, 116(D20), doi:10.1029/2011JD016076.

594 Lebsock, M. D., T. S. L'Ecuyer, and G. L. Stephens (2011), Detecting the Ratio of Rain
595 and Cloud Water in Low-Latitude Shallow Marine Clouds, *Journal of Applied*
596 *Meteorology and Climatology*, 50(2), 419–432, doi:10.1175/2010JAMC2494.1.

597 Lebsock, M., and H. Su (2014), Application of active spaceborne remote sensing for
598 understanding biases between passive cloud water path retrievals, *Journal of*
599 *Geophysical Research-Atmospheres*, 119(14), 8962–8979,
600 doi:10.1002/2014JD021568.

601 Liljegren, J. C., E. E. Clothiaux, G. G. Mace, S. Kato, and X. Dong (2001), A new
602 retrieval for cloud liquid water path using a ground-based microwave radiometer and
603 measurements of cloud temperature, *J. Geophys. Res.*, 106(D13), 14485–14500,
604 doi:10.1029/2000JD900817.

605 Loeb, N. G., S. Kato, K. Loukachine, and N. Manalo-Smith (2005), Angular Distribution
606 Models for Top-of-Atmosphere Radiative Flux Estimation from the Clouds and the
607 Earth's Radiant Energy System Instrument on the Terra Satellite. Part I:
608 Methodology, *J. Atmos. Oceanic Technol.*, 22(4), 338–351,
609 doi:10.1175/JTECH1712.1.

610 Logan, T., B. Xi, and X. Dong (2014), Aerosol properties and their influences on marine
611 boundary layer cloud condensation nuclei at the ARM mobile facility over the
612 Azores, *Journal of Geophysical Research-Atmospheres*, 119(8), 4859–4872,
613 doi:10.1002/2013JD021288.

614 Long, C. N., and T. P. Ackerman (2000), Identification of clear skies from broadband
615 pyranometer measurements and calculation of downwelling shortwave cloud effects,
616 *J. Geophys. Res.*, 105(D12), 15609–15626, doi:10.1029/2000JD900077.

617 Miller, D. J., Z. Zhang, A. S. Ackerman, S. Platnick, and B. A. Baum (2016), The impact
618 of cloud vertical profile on liquid water path retrieval based on the bispectral method:
619 A theoretical study based on large-eddy simulations of shallow marine boundary
620 layer clouds, *Journal of Geophysical Research-Atmospheres*, 121(8), 4122–4141,
621 doi:10.1002/2015JD024322.

622 Minnis, P. et al. (2011a), CERES Edition-2 Cloud Property Retrievals Using TRMM
623 VIRS and Terra and Aqua MODIS Data; Part II: Examples of Average
624 Results and Comparisons With Other Data, *IEEE TRANSACTIONS ON*
625 *GEOSCIENCE AND REMOTE SENSING*, 49(11), 4401–4430,
626 doi:10.1109/TGRS.2011.2144602.

627 Minnis, P. et al. (2011b), CERES Edition-2 Cloud Property Retrievals Using TRMM
628 VIRS and Terra and Aqua MODIS Data-Part I: Algorithms, *IEEE TRANSACTIONS*

- 629 *ON GEOSCIENCE AND REMOTE SENSING*, 49(11), 4374–4400,
630 doi:10.1109/TGRS.2011.2144601.
- 631 Minnis, P., R. Arduini, D. Young, and J. Ayers (2004), An Examination of the Impact of
632 Drizzle Drops on Satellite-Retrieved Effective Particle Sizes, ... of 14th International
633 Conference on Clouds and
- 634 Minnis, P., S. Sun-Mack, Y. Chen, M. M. Khaiyer, Y. Yi, J. K. Ayers, R. R. Brown, X.
635 Dong, S. C. Gibson, and P. W. Heck (2011c), CERES Edition-2 Cloud Property
636 Retrievals Using TRMM VIRS and Terra and Aqua MODIS Data—Part II:
637 Examples of Average Results and Comparisons With Other Data,, 49(11), 4401–
638 4430.
- 639 Nakajima, T. Y., K. Suzuki, and G. L. Stephens (2010), Droplet growth in warm water
640 clouds observed by the A-Train. Part I: Sensitivity analysis of the MODIS-derived
641 cloud droplet sizes,, 67(6), 1884–1896, doi:10.1175/2009JAS3280.1.
- 642 Nakajima, T., M. D. King, and J. D. Spinhirne (1990), Determination of the Optical
643 Thickness and Effective Particle Radius of Clouds from Reflected Solar Radiation
644 Measurements. Part I: Theory, *JAS*, 47(15), 1878–1893, doi:10.1175/1520-
645 0469(1990)047<1878:DOTOTA>2.0.CO;2.
- 646 Painemal, D., and P. Zuidema (2011), Assessment of MODIS cloud effective radius and
647 optical thickness retrievals over the Southeast Pacific with VOCALS-REx in situ
648 measurements, *J Geophys Res*, 116(D24), D24206.
- 649 Painemal, D., P. Minnis, and S. Sun-Mack (2013), The impact of horizontal
650 heterogeneities, cloud fraction, and liquid water path on warm cloud effective radii
651 from CERES-like Aqua MODIS retrievals, *ACP*, 13(19), 9997–10003,
652 doi:10.5194/acpd-13-12725-2013.
- 653 Painemal, D., P. Minnis, J. K. Ayers, and L. O'Neill (2012), GOES-10 microphysical
654 retrievals in marine warm clouds: Multi-instrument validation and daytime cycle over
655 the southeast Pacific, *J Geophys Res*, 117(D19), D19212,
656 doi:10.1029/2012JD017822.
- 657 Pincus, R., S. Platnick, S. A. Ackerman, R. S. Hemler, and R. J. Patrick Hofmann (2012),
658 Reconciling simulated and observed views of clouds: MODIS, ISCCP, and the limits
659 of instrument simulators, *Journal of Climate*, 120220120058001, doi:10.1175/JCLI-
660 D-11-00267.1.
- 661 Platnick, S. (2000), Vertical photon transport in cloud remote sensing problems, *Journal*
662 *of Geophysical Research*, 105(D18).
- 663 Platnick, S. et al. (2016), The MODIS Cloud Optical and Microphysical Products:
664 Collection 6 Updates and Examples From Terra and Aqua, *IEEE TRANSACTIONS*
665 *ON GEOSCIENCE AND REMOTE SENSING*, 55(1), 502–525,
666 doi:10.1109/TGRS.2016.2610522", "rightsLink": "http://s100.copyright.com/AppDisp

atchServlet?publisherName=ieee&publication=0196-
2892&title=The+MODIS+Cloud+Optical+and+Microphysical+Products%3A+Colle
ction+6+Updates+and+Examples+From+Terra+and+Aqua&isbn=&publicationDate
=Jan.+2017&author=Steven+Platnick&ContentID=10.1109/TGRS.2016.2610522&o
rderBeanReset=true&startPage=502&endPage=525&volumeNum=55&issueNum=1"
,"displayPublicationTitle": "IEEE.

Platnick, S., M. D. King, S. A. Ackerman, W. P. Menzel, B. A. Baum, J. C. Riédi, and R.
A. Frey (2003), The MODIS cloud products: algorithms and examples from Terra,
IEEE TRANSACTIONS ON GEOSCIENCE AND REMOTE SENSING, 41(2), 459–
473, doi:10.1109/TGRS.2002.808301.

Seethala, C., and Á. Horváth (2010), Global assessment of AMSR-E and MODIS cloud
liquid water path retrievals in warm oceanic clouds, *J Geophys Res*, 115(D13),
D13202.

Wood, R. (2012), Stratocumulus Clouds, *Mon. Wea. Rev*, 140(8), 2373–2423,
doi:10.1175/MWR-D-11-00121.1.

Wood, R. et al. (2014), Clouds, Aerosol, and Precipitation in the Marine Boundary Layer:
An ARM Mobile Facility Deployment, <http://dx.doi.org/10.1175/BAMS-D-13-00180.1>, 140617093021002, doi:10.1175/BAMS-D-13-00180.1.

Xi, B., X. Dong, P. Minnis, and S. Sun Mack (2014), Comparison of marine boundary
layer cloud properties from CERES-MODIS Edition 4 and DOE ARM AMF
measurements at the Azores, *Journal of Geophysical Research-Atmospheres*,
119(15), 9509–9529, doi:10.1002/2014JD021813.

Zhang, Z., A. S. Ackerman, G. Feingold, S. Platnick, R. Pincus, and H. Xue (2012),
Effects of cloud horizontal inhomogeneity and drizzle on remote sensing of cloud
droplet effective radius: Case studies based on large-eddy simulations, *J Geophys
Res*, 117(D19), D19208–, doi:10.1029/2012JD017655.

Zhang, Z., and S. Platnick (2011), An assessment of differences between cloud effective
particle radius retrievals for marine water clouds from three MODIS spectral bands, *J
Geophys Res*, 116(D20), D20215, doi:10.1029/2011JD016216.

697 **Figures and Tables:**

698

699 Table 1 Correlation coefficient between ground-based LWP retrievals from MWR and satellite-
700 based LWP retrievals from GSFC-MODIS product for different collocation strategies

	dL=30 km	dL=20 km	dL=10 km
dt = 60 min	0.62 (0.63)	0.66 (0.67)	0.71 (0.73)
dt = 30 min	0.66 (0.67)	0.72 (0.73)	0.77 (0.78)
dt = 10 min	0.75 (0.75)	0.79 (0.79)	0.84 (0.85)

701

703

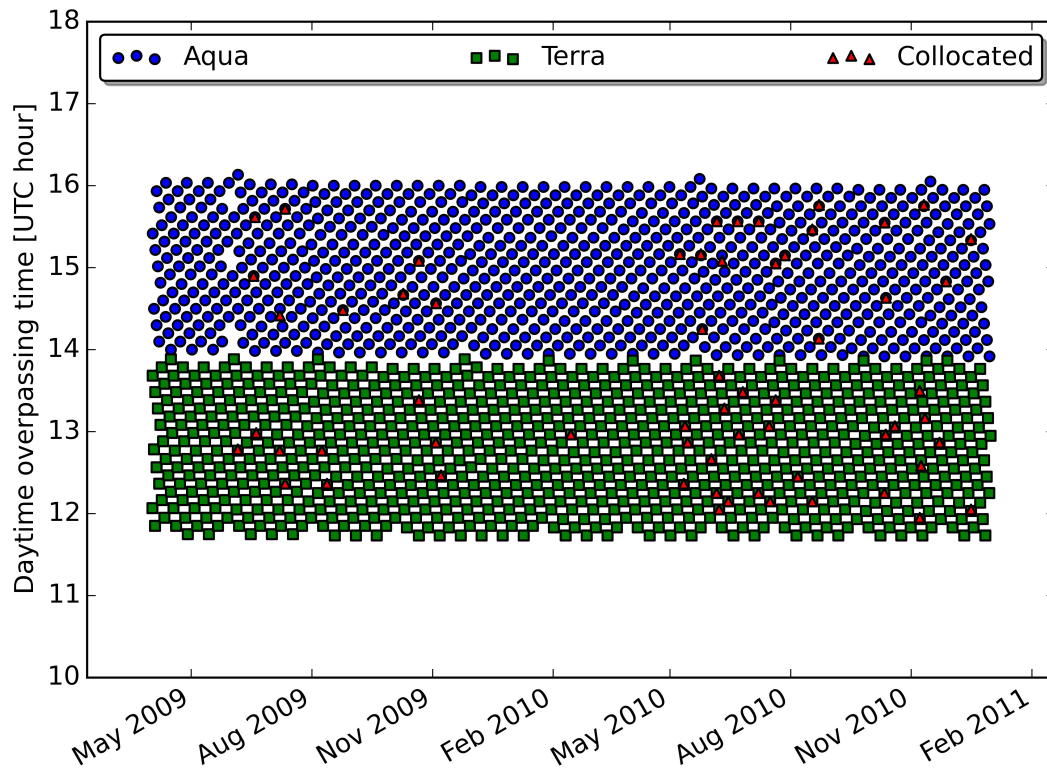
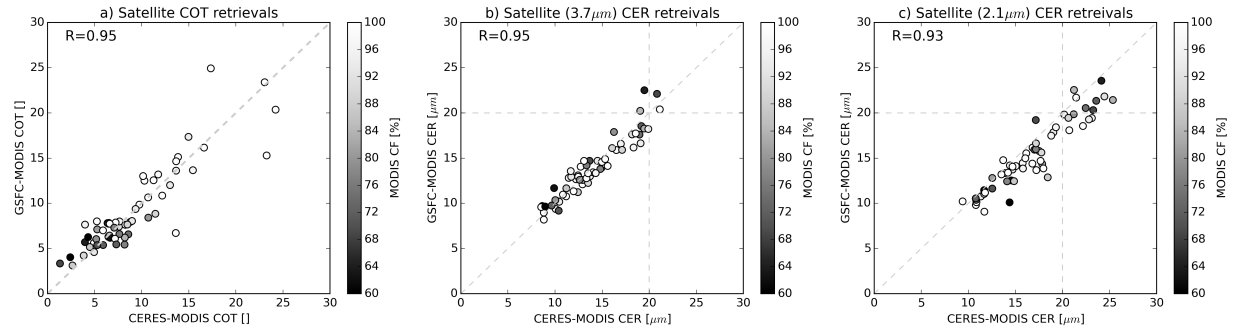


Figure 1. MODIS swath overpass times for Graciosa Island ($39^{\circ} 5' 28''$ N, $28^{\circ} 1' 45''$ W) during the CAP-MBL campaign. Blue dots (Aqua) and green squares (Terra) indicate MODIS swath overpass times. Red triangles mark the 63 daytime collocated cases in *Xi et al.* [*Xi et al.*, 2014].

709



710

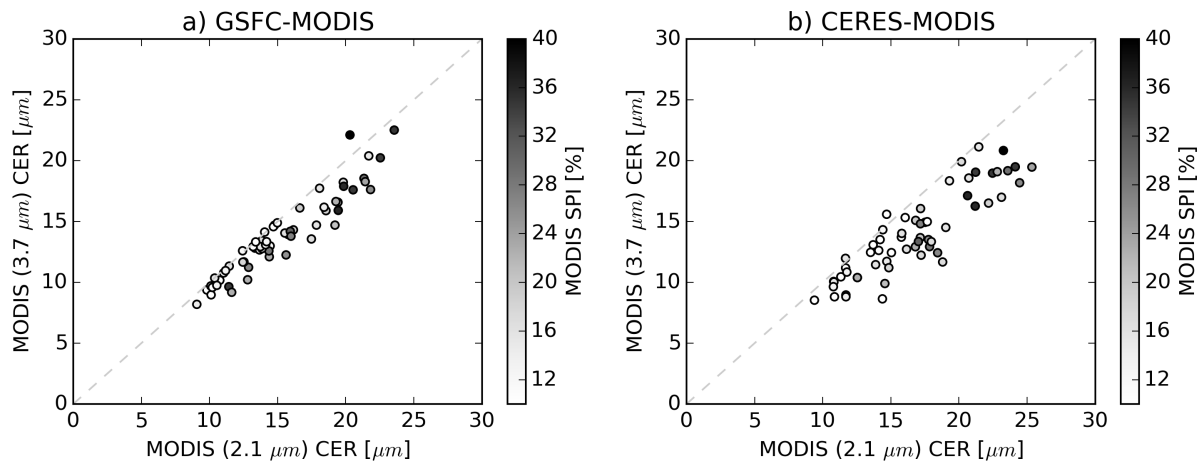
711

712 **Figure 2.** Comparison of a) COT, b) CER_{2.1} and c) CER_{3.7} of MBL clouds between collocated
713 the CERES-MODIS and GSFC-MODIS products for the 63 selected cases in Xi14.

714

715

716

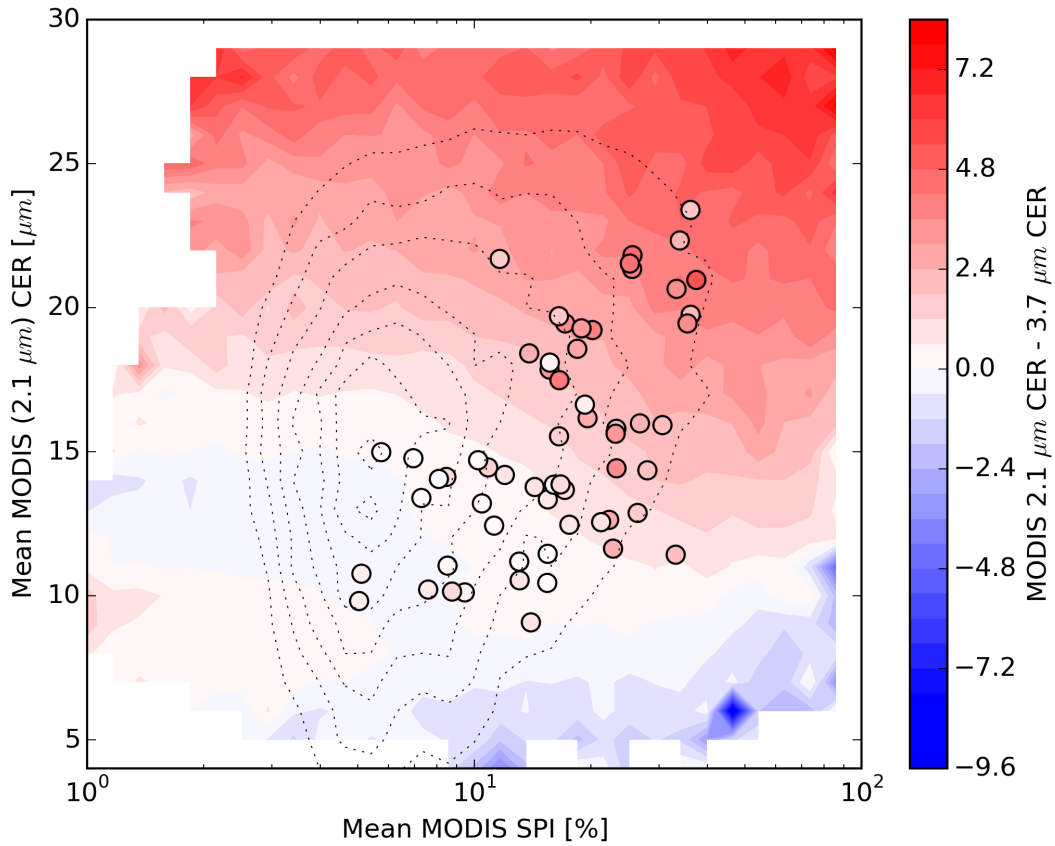


717

718 **Figure 3.** Comparison between $\text{CER}_{2.1}$ and $\text{CER}_{3.7}$ in a) GSFC-MODIS and b) CERES-MODIS
719 cloud products for the 63 selected cases.

720

721

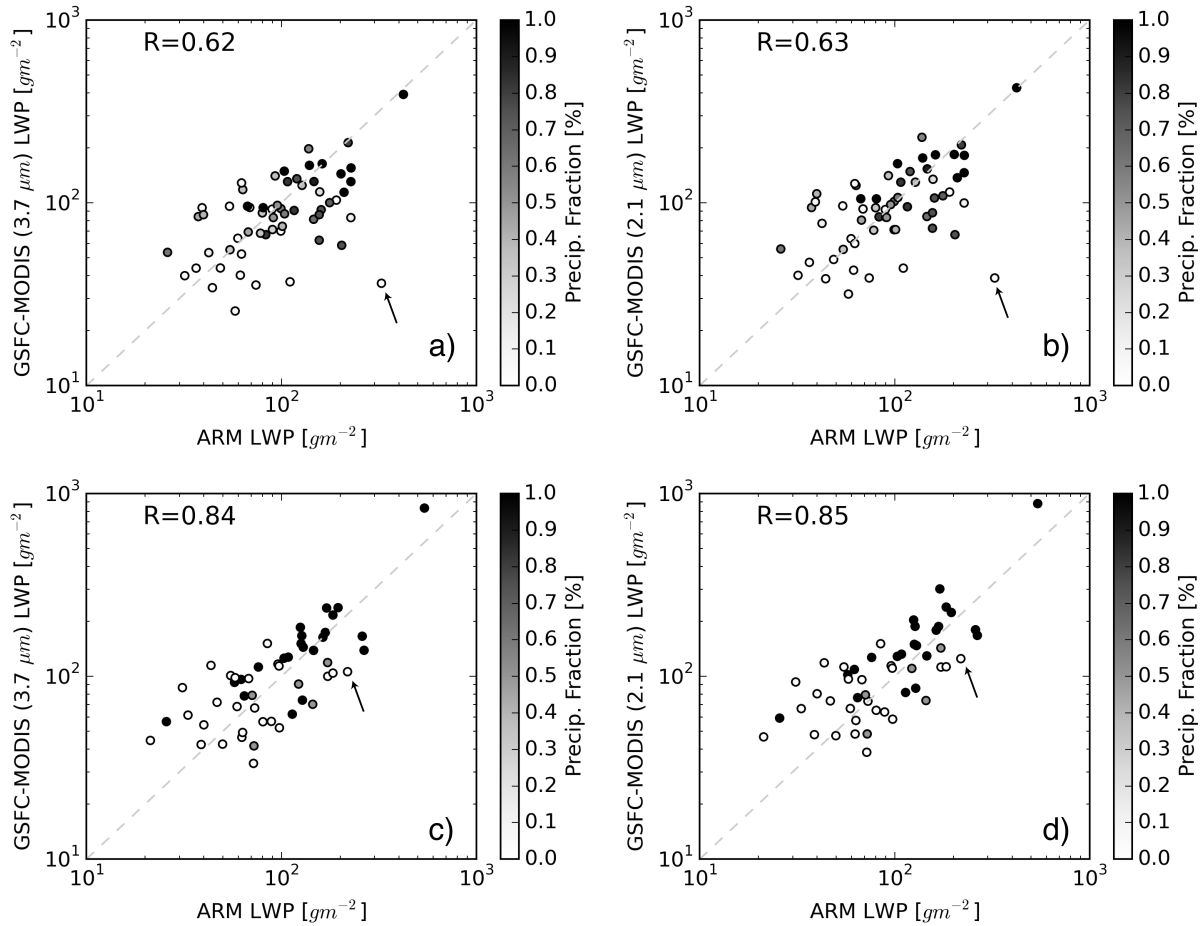


722

723 **Figure 4.** A composite plot of $CER_{2.1}-CER_{3.7}$ as a joint function of MODIS sub-pixel
 724 inhomogeneity index (SPI) and $CER_{2.1}$. The background color map corresponds to the mean
 725 $CER_{2.1}-CER_{3.7}$ at each pair of SPI index and $CER_{2.1}$ derived from the total population of GSFC-
 726 MODIS pixels for all 63 cases. The dotted contour lines correspond to the sampling rate. Each
 727 dot in the figure corresponds to one of the 63 cases. The location of the dots on x- and y-axis
 728 corresponds to the mean value of SPI index and $CER_{2.1}$ of each case, respectively. The color of
 729 each dot corresponds to the mean $CER_{2.1}-CER_{3.7}$ of each case.

730

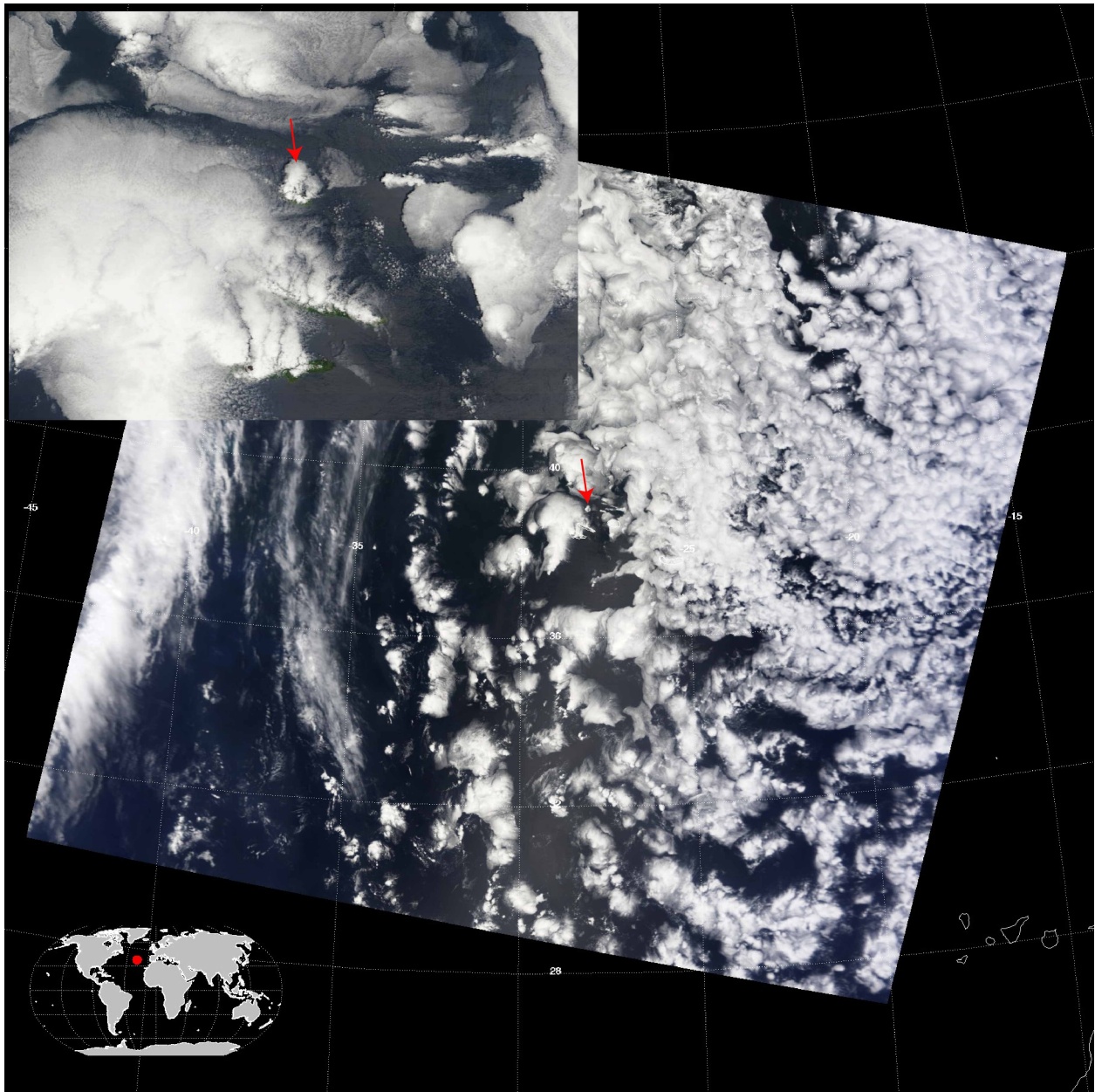
731



732

733 **Figure 5.** Comparisons of ground-based LWP retrievals from MWR with the GSFC-MODISa)
 734 LWP_{2.1} and b) LWP_{3.7} products using the dL30km-dt60min averaging scheme. C-d) are same as
 735 a-b) except for the averages from the dL10km-dt10min scheme. Gray scale of the dots
 736 corresponds to the fraction of precipitating MBL clouds during the temporal averaging window
 737 according to the ARM ground-based MMCR observations. The small arrow in the figure marks
 738 the May 14th, 2010 case (see **Figure 6** and text for details).

739



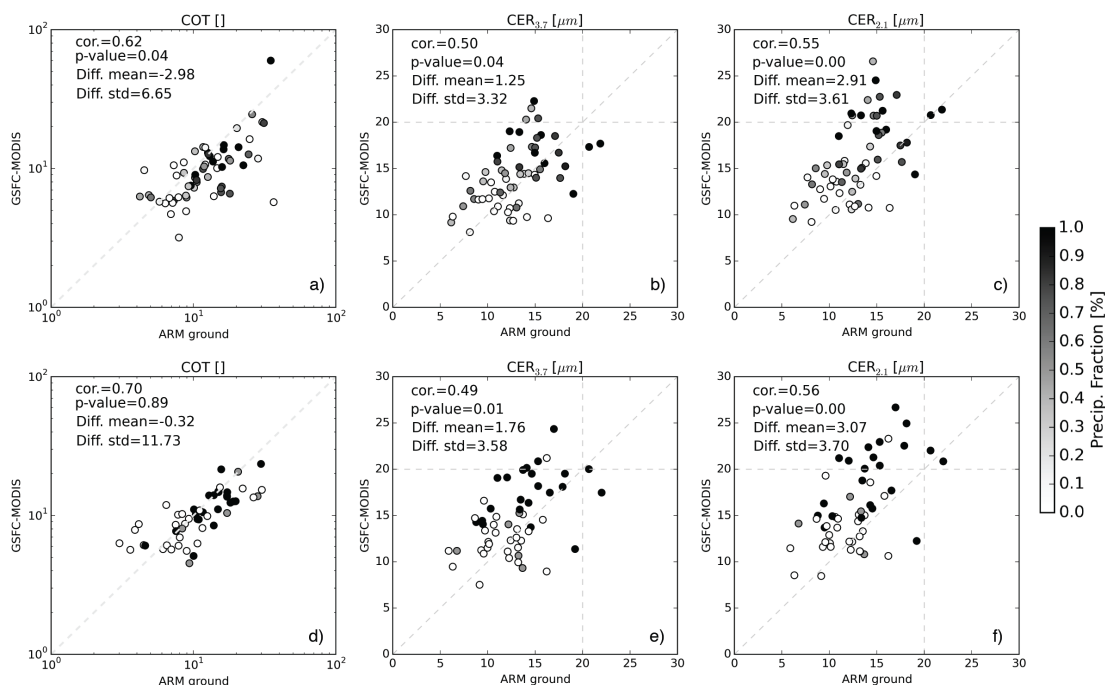
741

742 **Figure 6.** The RGB image from Terra-MODIS for the May 14th, 2010 case. The red arrow
743 indicates the island of Graciosa (39.09°N, 28.03°W) where the ARM AMF is located.

744

745

746



747

748 **Figure 7.** Comparisons of (a) COT, (b) CER_{2.1} and (c) CER_{3.7} from GSFC-MODIS cloud
 749 product with the ground-based retrievals based on *Dong et al.* [1998] algorithm under the
 750 dL30km-dt60min averaging scheme. (d-f) are same as (a-c) expect for averaging based on
 751 dL10km-dt10min scheme.

752

753

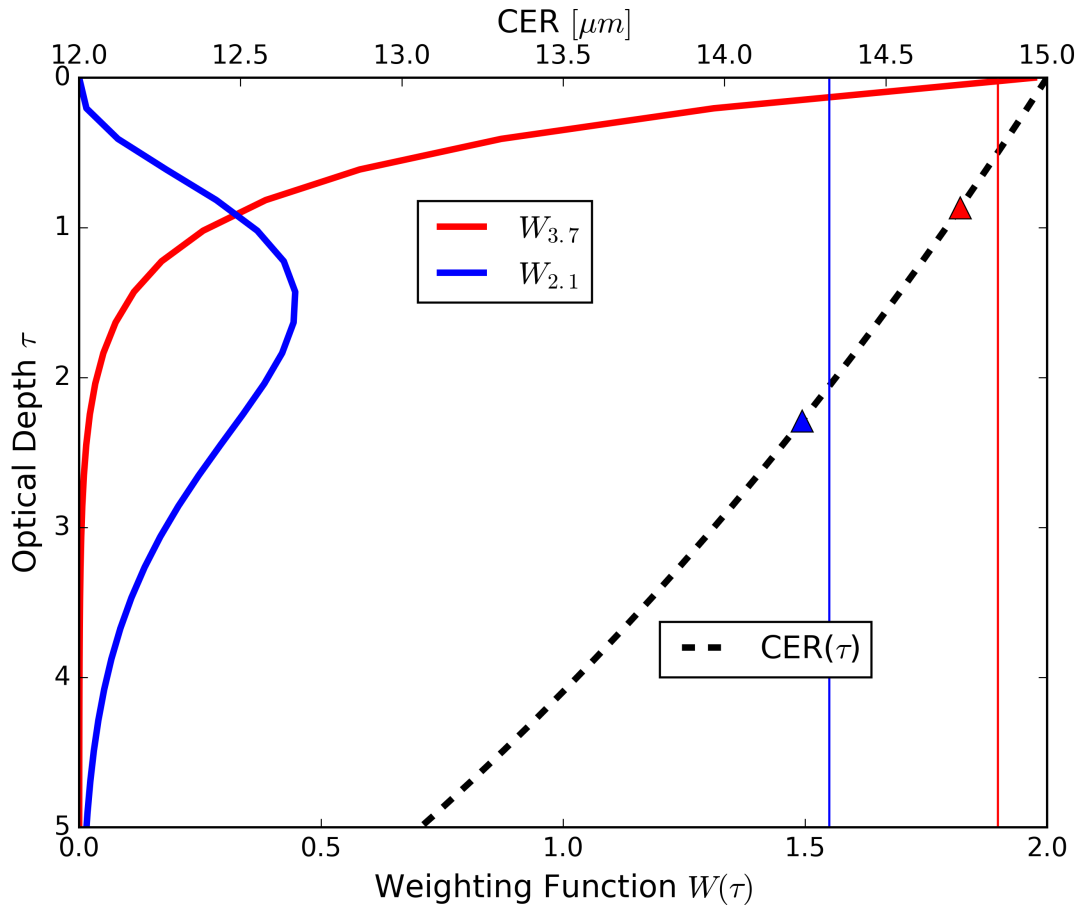


Figure 8. Schematic diagram to illustrate the vertical distributions of CER and COT from two MODIS bands. The red and blue solid curves are the weighted COTs $W(\tau)$ for $\text{CER}_{3.7}$ and $\text{CER}_{2.1}$ retrievals, respectively. The dashed black curve corresponds to an adiabatic CER profile with the $\text{CER}=15 \mu\text{m}$ at cloud top. The red and blue triangles mark the $\text{CER}_{3.7}$ and $\text{CER}_{2.1}$ retrievals from theoretical calculations. The red and blue vertical lines mark the locations of the retrieved $\text{CER}_{3.7}$ and $\text{CER}_{2.1}$ predicted by the weighting function in Eq.. In this case $\mu = \mu_0 = 1$, the total $\text{COT}=10$ and the CER profile follows the classic adiabatic structure.

765

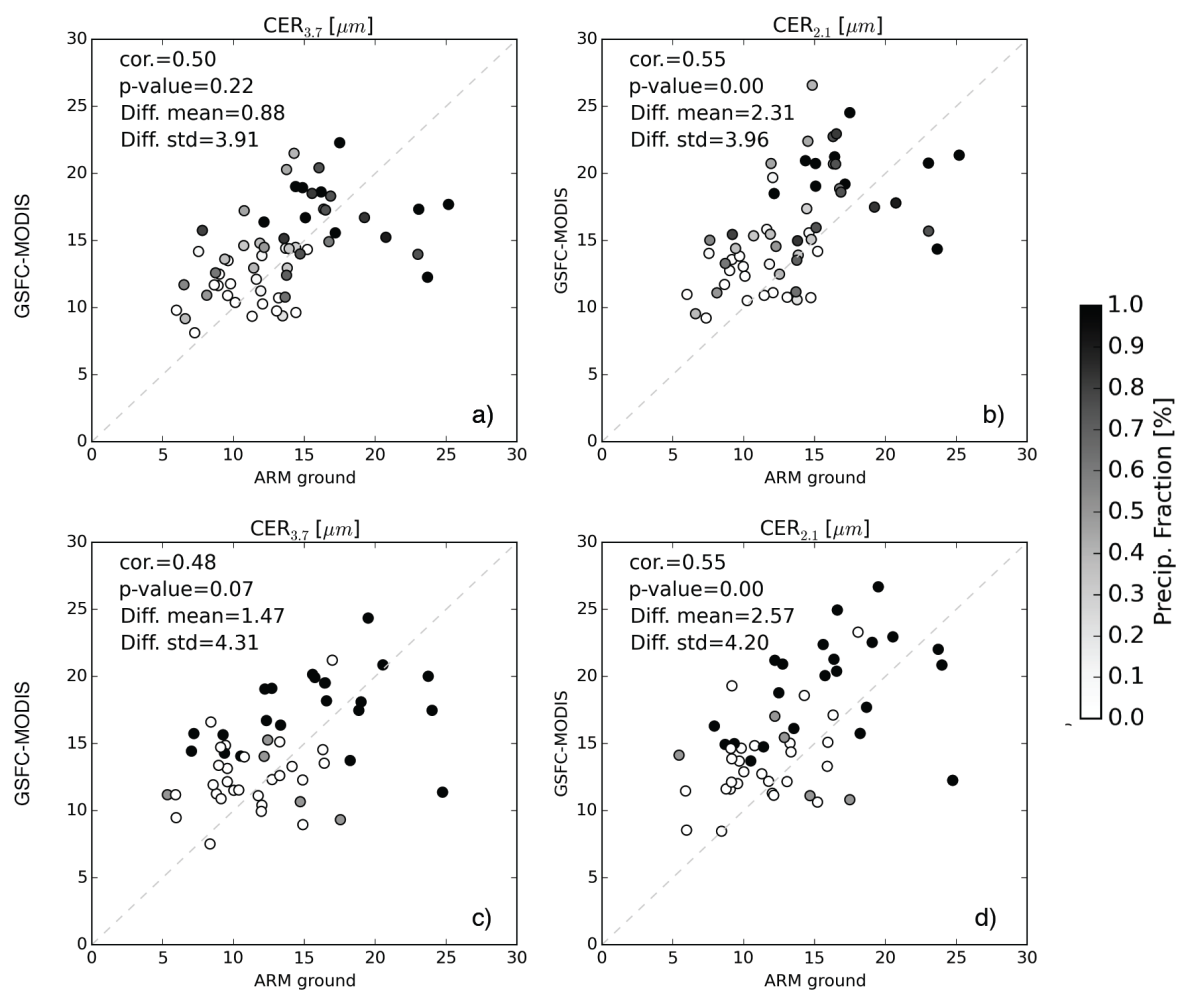


Figure 9. Same as **Figure 7**, except that the ground-based CER retrievals are vertically weighted results using the analytical weighing function in Eq. and the LWC and CER profile from *Dong and Mace* [2010] algorithm.

